Recommended Citation (primary publication/Version of Record) incl. DOI:

Take down policy
If you believe that this document or any material on this site infringes copyright, please contact publizieren@suub.uni-bremen.de with full details and we will remove access to the material.

A physical explanation of the gas flow diode effect

I. Graur[1] ⬤ · **J. G. Méolans**[1] · **P. Perrier**[1] · **J. Thöming**[2] · **T. Veltzke**[2]

Abstract Gas flow properties in channels with slightly varying cross section have a dependency on the direction of channel perfusion when the gas is in the slip and transitional flow regimes. In the past, it was observed that the flow rate in converging direction is higher compared to the case where the channel diverges alongside. This gas flow diode effect does neither exist in the continuum regime nor in the free molecular regime, and it has its maximum at the same level of gaseous rarefaction as the well-known Knudsen minimum. However, no comprehensive study on the physics of this diode effect is carried out yet. In order to overcome this knowledge gap, the current paper proceeds our previous works by an appropriate experimental study. Here we can show that the diode effect crucially depends on the proportion of inclined walls to the overall channel inner surface. Also the inclination of the wall itself determines the strength of the diode effect meaning that the diodicity increases with the opening angle. Furthermore, we found indication that the diodicity also depends on the molar mass and the internal structure of the impinging gas molecules. Finally, we propose an explanation of the diode effect that is mainly based on the tangential reflection process of gas molecules colliding with the inclined walls of a tapered channel.

✉ I. Graur
  irina.martin@univ-amu.fr

[1] Aix-Marseille Université, CNRS, IUSTI UMR 7343,
   13453 Marseille, France

[2] Center for Environmental Research and Sustainable
   Technology (UFT), University of Bremen,
   Leobener Strasse 1, 28359 Bremen, Germany

1 Introduction

With the rapid development of microelectromechanical systems (MEMS), the knowledge on gas flows through channels of different cross-sectional shapes becomes very important for handling and manipulating gaseous microflows for, e.g., analytical and medical applications. Additionally, such flows are an exciting and challenging problem of fundamental fluid mechanics. In particular, in the transitional flow regime, where neither intermolecular collisions nor molecule–wall collisions dominate the flow behavior, strong deviation from either continuum theory or free molecular theory is observed.

While rarefied gas flows in uniform ducts have been widely investigated by means of analytical (e.g., Knudsen 1909; Lund and Berman 1966a; Arkilic et al. 2001; Graur et al. 2006), numerical (e.g., Sharipov and Seleznev 1994; Sharipov 1999; Barisik and Beskok 2014) and experimental (e.g., Lund and Berman 1966b; Ewart et al. 2007; Marino 2009; Varoutis et al. 2009; Velasco et al. 2012) approaches, only few studies were carried out on flows through conical tubes or tapered channels (Aubert et al. 1998; Sharipov and Bertoldo 2005; Veltzke et al. 2012; Titarev et al. 2013; Graur and Ho 2014; Varade et al. 2014; Graur et al. 2015; Varade et al. 2015; Hemadri et al. 2016). In our previous paper (Graur et al. 2015), we reported the gas flow diode effect, meaning a dependency of the mass flow rate on the direction of perfusion, that occurs in the slip and transitional flow regimes and is inexistent in the continuum regime. In the free molecular regime, this effect should not exist too, as it was claimed from numerical investigations (Sharipov and Bertoldo 2005; Graur and Ho 2014). Consequently, the diodicity has a maximum in the transitional flow regime, which was shown numerically by solving the

linearized BGK kinetic equation (Szalmas et al. 2015). In this flow regime, neither molecule–molecule c ollisions nor molecule–wall collisions are dominating. Other interesting phenomena occur in transitional flow regime as the Knusdsen minimum of the dimensionless mass flow rate in the pressure driven Poiseuille flow (Knudsen 1909; Steckelmacher 1986; Cercignani 1990), or the maximum of the thermal molecular pressure difference in the temperature gradient driven flows (Rojas-Cardenas et al. 2013; Yamaguchi et al. 2014).

Resuming the previous studies, one can conclude that no comprehensive study on the physics of the gas flow diode effect is carried out yet. Aiming to close this knowledge gap, the current paper proceeds and extends our previous works (Veltzke et al. 2012; Veltzke 2013; Graur et al. 2015; Szalmas et al. 2015) with an appropriate experimental study and with a physical explanation. First, the experimental results obtained on four totally different tapered channels are presented and analyzed in order to elaborate some basic consequential hypotheses. Then, we present and discuss a physical explanation of the diode effect, which takes into account the previous hypotheses and which is mainly based on the exchange and reflection process of the gas molecules at the channel walls.

2 Experimental results and discussion

2.1 Test channels

In the present study, four different types of test channel were used, which are referred to as Type A, B, C, and D, see Fig. 1. The channels of Type A and D are manufactured by means of milling a long notch into a piece of aluminum using raster fly-cutting. As it is shown schematically in Fig. 1a, d, the notch was capped with another plain piece of aluminum with high-quality optical surface. Both parts were screwed together and sealed by means of the perfectly plain surfaces. All parts were manufactured by the LFM (Laboratory for Precision Machining, University of Bremen) using a Nanotech 350FG (Moore Nanotechnology Systems, Keene, NH, USA). The tapered channel with alongside varying rectangular cross section (Type A) has a constant width, w, that is much larger than the height, h,
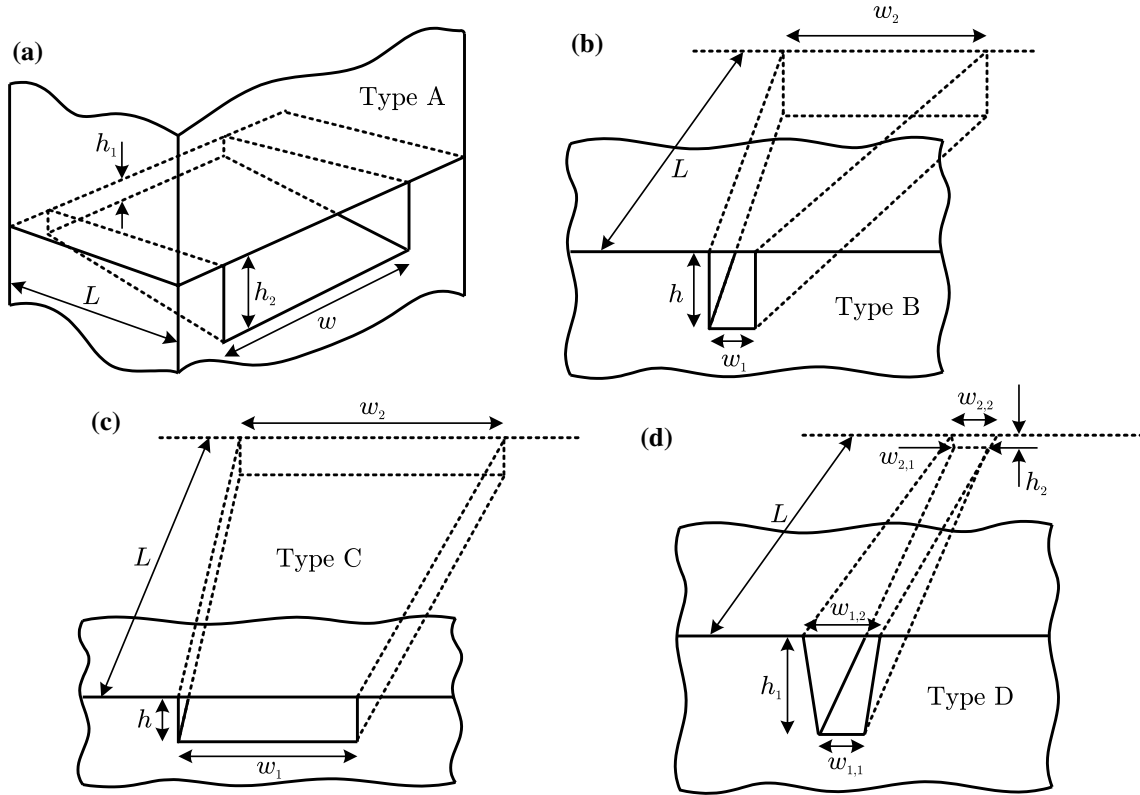
Fig. 1 Four different types of tapered channels. The Type A channel has $h_1 < h_2 \ll w$ (**a**) while the Type B channel has $w_1 < h < w_2$ (**b**). The Type C channel has $h \ll w_1 < w_2$ being the third type of channel with a rectangular cross section. The fourth channel, Type D, has a trapezoidal cross section with $h_2 < w_{1,1}, w_{2,1} < w_{2,2} < w_{1,2} < h_1$ (**d**). For all channels, the length L is much larger than the other dimensions so that the *long channel assumption* is fulfilled

Table 1 Test channel dimensions and details

Channel	Length L (μm)	Small width w_1 (μm)	Large width w_2 (μm)	Small height h_1 (μm)	Large height h_2 (μm)	Roughness ς (nm)	Number k (–)
Type A	11050	1007.5	1007.5	0.96	252.8	73	1
Type B	15000[a]	2.2	22.1	9.0	9.0	9.8	945[b]; 429[c]
Type C	12060	50[a]	350[a]	7.715	7.715	11.3	1
Type D	12000[a]	101.81; 102.01	101.81; 162.91	312.79	1.0[a]	$\approx$70	27

k is the number of parallel channels

[a] Nominal value

[b] Calorimetric mass flow sensing

[c] Constant volume measurements

which varies alongside the channel ($h_1 < h < h_2 \ll w$). The Type D channel has a trapezoidal cross section whereby the height h_1 at the one side is larger than the corresponding widths ($w_{1,1}$ and $w_{1,2}$), and the height h_2 at the opposite position is lower than the widths ($w_{2,1}$ and $w_{2,2}$). In case of Type D in total 27 parallel channels were fabricated in order to enhance the mass flow rate to be measured with the technique used (see Sect. 2.2).

The channels of Type B and C are produced by means of deep-reactive ion etching (DRIE) by the Institute for Microsensors, -Actuators and -Systems (IMSAS) at University of Bremen. As a substrate, a double side polished Si(100) wafer with a thickness of 380 μm was used. First, a mask with the structure was produced by a photo-lithography method. By using the mask, the microstructures (channels) were etched with an etching rate of approximately 2 μm per minute. Finally, a wet chemical cleaning was done with Caro's acid (sulfuric acid with hydrogen peroxide). This is a standard procedure, and more details can be found in Franssila (2010). After etching and cleaning the microchannels, measurements of etching depth (channel height h) and surface roughness ζ were taken by using the optical measuring and analysis system (UBM KF3 with software UBSoft 1.9). The measuring range was ±50 μm. Over a measuring path with a length of 0.56 mm 560 points were acquired. Finally, the arithmetic mean of h and the roughness were calculated. Afterward, the channels were sealed by anodic bonding a 500 μm thick capping wafer of double side polished borosilicate glass onto the top of the channel wafer. The bonded wafer was finally diced into smaller chips for handling, thus completing the fabrication sequence.

In case of Type B in total 945 (for calorimetric mass flow sensing, Sect. 2.2) and 429 (for constant volume measurements, Sect. 2.2), parallel channels were fabricated in order to enhance the mass flow rate. This channel type has the specification that the constant height is lower than the width at the one side but higher than the width at the

opposite side ($w_1 < h < w_2$). The Type C, that comprises only one single channel, is different again: here the height is constant too, but always much lower than both widths ($h \ll w_1 < w_2$).

The exact dimensions (including surface roughness and number of parallel channels) of all four channel types are stated in Table 1.

2.2 Mass flow rate measurements

All mass flow rate measurements were taken under isothermal conditions using two different experimental techniques: the constant volume method (Ewart et al. 2006, 2007; Perrier et al. 2011a) and a commercially available calorimetric mass flow sensor (MFS) (Veltzke 2013; Graur et al. 2015). All details about the experimental setups, the acquisition and analysis of data, and the measuring ranges and uncertainties are provided in Refs. Ewart et al. (2006), Ewart et al. (2007), Perrier et al. (2011a), Veltzke (2013), Graur et al. (2015). The conditions and specifications of mass flow rate measurements, considered in this work, are summarized in Table 2. The raw data obtained on the Type A channel can be also found in Ref. Graur et al. (2015). For each channel, the same type of measurements are carried out, which allow to associate the measured mass flow rate with corresponding couple of pressures, p_1 and p_2, at each channel end ($p_1 > p_2$). All measurements are taken in both, nozzle and diffusor, directions for each channel.

Table 2 Experimental conditions and methods used

Channel	Temperature (K)	Gas	Method
Type A	293.2	N_2, Ar, CO_2	Calorimetric MFS
Type B	294.6	CO_2	Calorimetric MFS
	297.7	He	Constant volume
Type C	296.4	He	Constant volume
Type D	294.0	N_2, CO_2, N_2–H_2	Calorimetric MFS

2.3 Useful expressions for mass flow rate

To account for the extremely different channel specifications and geometries (see Fig. 1; Table 1) the hydraulic diameter, $D = 4A/P$, is chosen as a reference value (A is the cross-sectional area, and P is the perimeter). The formulas for hydraulic diameter D of the four channel types are provided in Table 4 in "Appendix" section. For a tapered channel, the hydraulic diameter varies alongside the channel; therefore, its minimum value, D_{min}, is chosen as the characteristic length of the flow. In order to allow for comparison between the four different channel types in terms of gaseous rarefaction a first dimensionless quantity, the mean Knudsen number Kn_m, is defined as

$$Kn_m = \frac{\lambda_m}{D_{min}}, \tag{1}$$

where λ_m is the molecular mean free path, defined here in the framework of the Variable Hard Sphere (VHS) model (Bird 1994) as:

$$\lambda_m = k_\lambda \frac{\mu}{p_m} \sqrt{\frac{2\mathcal{R}T}{\mathcal{M}}}, \tag{2}$$

where $p_m = 0.5(p_1 + p_2)$ is the mean pressure, $\mathcal{R}$ is universal gas constant, T is the temperature, $\mathcal{M}$ is the gas molar mass, $k_\lambda = (7 - 2\omega)(7 - 2\omega)/(15\sqrt{\pi})$ is the coefficient which is used in the VHS definition of the molecular mean free path, and ω is the gas viscosity index (Bird 1994). The viscosity μ is given in terms of the VHS model (Bird 1994) by a power-law function of the temperature

$$\mu = \mu_{ref} \left(\frac{T}{T_{ref}} \right)^\omega, \tag{3}$$

with μ_{ref} being the viscosity coefficient at the reference temperature, $T_{ref} = 273.15$ K. Here it is worth emphasizing that, in contrast to common fashion, we defined the Knudsen number by using the mean pressure and the hydraulic diameter in order to allow for the comparison of various experimental data.

To compare the tapered channels with various cross-sectional aspect ratios, we introduced above the hydraulic diameter, and now we define the dimensionless mass flow rate, based on this hydraulic diameter instead of the tube diameter as in Ref. Ewart et al. (2007). In case, this hydraulic diameter varies alongside the channel, its minimum value, D_{min}, is used (as it was done for the definition of the Knudsen number) in the dimensionless mass flow rate definition:

$$G = \frac{L}{k(p_1 - p_2)\pi D_{min}^3} \sqrt{\frac{2\mathcal{R}T}{\mathcal{M}}} \dot{M}. \tag{4}$$

In Eq. (4) $\dot{M}$ is the dimensional mass flow rate in (kg/s), and k is the number of parallel channels, see Table 1.

It is worth emphasizing that the dimensionless mass flow rate $\dot{M}/(p_m^2(0.5h_1)^3 w/(\mu RTL))$ through converged/diverged channel in the hydrodynamic and slip regimes can be presented [see Eqs. (18) and (21) in Ref. Graur et al. 2015] as a series of the Knudsen number. We define here another dimensionless mass flow rate G, see Eq. (4), which varies also as a function of the mean pressure in a channel and, therefore, of the Knudsen number. Since it was experimentally impossible to adjust exactly the same mean Knudsen number, we fitted the mass flow rate G of each data set as function of the mean Knudsen number in order to compare the mass flow rate in two directions of perfusion reliably and precisely. For the fitting of the dimensionless mass flow rate, G, we use as previously the following polynomial form in Knudsen number

$$G_F = \frac{a}{Kn_m} + b + cKn_m, \tag{5}$$

here a, b, and c are the fitting coefficients. It is worth to note that the form of fitting, Eq. (5), corresponds to the asymptotic expansion of the mass flow rate through a channel of a constant cross-sectional area, see Ref. Sharipov and Seleznev (1998). The approach based on the Navier–Stokes equation with the slip boundary condition at the channel walls allows us to obtain the terms of the order of $O(1/Kn_m)$ and $O(1)$ in the mass flow rate expansion according to the Knudsen number. Using the integro-moment method (Sharipov and Seleznev 1998) we may find more terms in this expansion, see Eq. 5.

To develop a quantitative measure of the diode effect, we define the diodicity as the ratio between the dimensionless mass flow rates in the nozzle and diffusor directions as

$$\mathcal{D} = \frac{G_F^{noz}}{G_F^{dif}}, \tag{6}$$

where G_F^{noz} and G_F^{dif} are the dimensionless expressions of the experimental mass flow rate in nozzle and diffusor directions, respectively, fitted according to Eq. (5).

2.4 Experimental mass flow rate results

All experimental results on the mass flow rate, obtained by the $\dot{M}$ measurements, following Sect. 2.2, are shown in Fig. 2 in the dimensionless form G, Eq. (4), versus mean Knudsen number Kn_m, defined by Eq. (1). These data are obtained for four channels and for both, nozzle and diffusor, perfusion directions indicated with filled and open symbols. The required properties of the test gases are provided in Table 5 in "Appendix" section. The values of $\mathcal{M}$

(a) Channel Type A

(b) Channel Type B

(c) Channel Type C

(d) Channel Type D
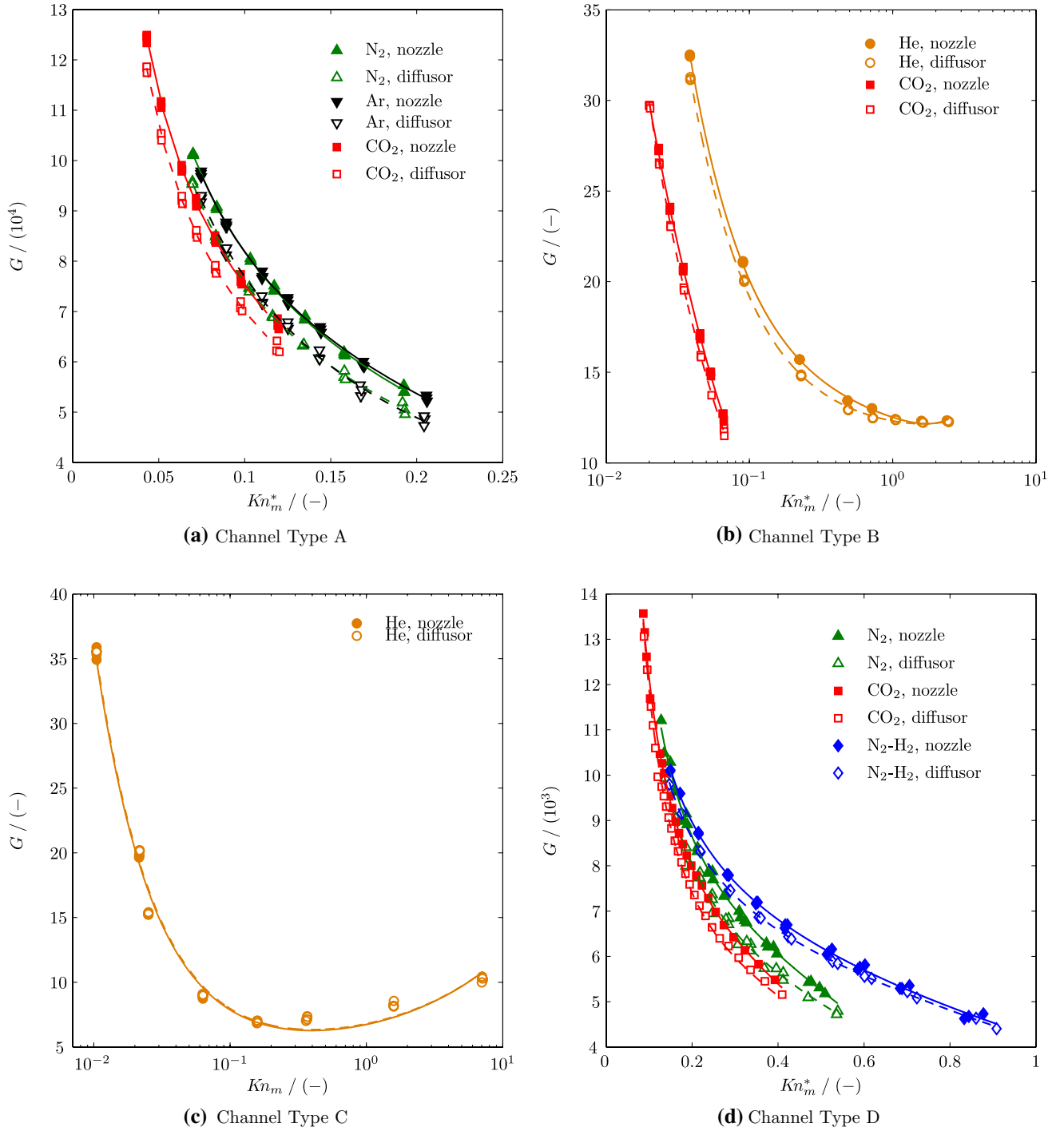
Fig. 2 Experimental results on the mass flow rate depicted in nondimensional form, G, Eq. (4), versus the Knudsen number Kn_m, Eq. (1). The curves are fitted to the data using the fitting function according to Eq. (5). *Solid curves* and *filled symbols* represent the nozzle direction, and *dashed curves* and *open symbols* represent the diffusor direction

and ω of the nitrogen–hydrogen gas mixture (50–50 mol%) are taken as the arithmetic mean of the values of pure nitrogen and pure hydrogen. The reference viscosity μ_{ref} of the mixture is calculated as stated by Wilke (1950) under the assumption of ideal gas behavior.

The experimentally obtained mass flow rate was also fitted according Eq. (5). These curves are shown also in Fig. 2 as solid lines for the nozzle direction and as dashed lines for the diffusor direction, each matching the experiments very well. The determination coefficients were always at least 0.97.

Table 3 Calculated properties of test channels

Channel	D_1 (μm)	D_2 (μm)	Φ (–)	α (°)
Type A	1.92	404.18	0.888	1.0428
Type B	3.54	12.79	0.426	0.0177
Type C	13.37	15.09	0.037	0.0041
Type D	1.98	185.39	–	0.4378

Hydraulic diameters are calculated according to formulas given in Table 4 in "Appendix" section. The ratio of inclined to the overall wall surface Φ, and the opening angle α are calculated according to Eqs. (8) and (9), respectively

The results obtained for the Type A channel (Fig. 2a) clearly indicate that the mass flow rate in converging direction (nozzle) is significantly higher than in diverging direction (diffusor). This is true for all three gases that were used for the mass flow rate measurements. The same tendency is observed for all test gases used in experiments with the channels of Type B and D (Fig. 2b, d). Only the channel of Type C (Fig. 2c) does not show any influence of the perfusion direction.

The absence of the diode effect of the Type C channel can be related to the fact that the (small) channel height is constant along the channel and the geometry resembles the parallel plate configuration. In Ref. Méolans et al. (2012), it was shown that for the width-to-height ratio equal to 5, the mass flow rate is different from the mass flow rate between two parallel plates (very broad channel) in 12 %, while when this ratio is equal to 50, the corresponding difference is reduced to 1.2 %. Therefore in this channel geometry, Type C, the influence of the inclined walls becomes really negligible.

The influence of the ratio between inclined wall surface and total wall surface to the diode effect is discussed in the next Section.

2.5 Proportion of inclined surfaces

In order to relate more clearly the effect of the inclined surface on the diode effect, we define the ratio between the areas of the inclined and total surfaces of the channel walls as

$$\Phi = \frac{A_{\text{inc}}}{A_{\text{S}}}, \tag{7}$$

where A_{inc} and A_{S} are the areas of the inclined and total surfaces of the channel walls, respectively.

With the introduced definition, Eq. (7), for the Type C channel the part of inclined surface is
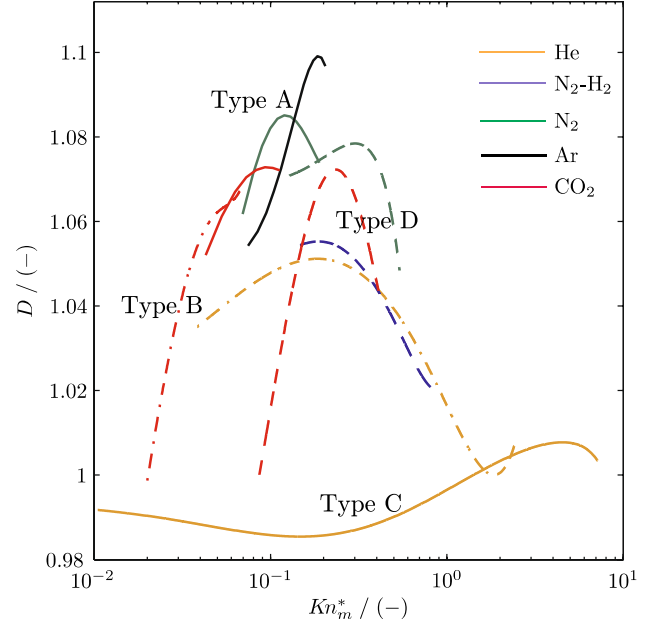
Fig. 3 Diodicity, according to Eq. (6), versus the Knudsen number Kn_{m}, defined by Eq. (1). Results for channels of Type A and C are indicated by *solid lines* while Type B is represented by *dot-dashed lines* and Type D by *dashed ones*. The different test gases are indicated by the particular *colors* according to the legend

$$\Phi = \frac{A_{\text{inc}}}{A_{\text{S}}} = \frac{2h\sqrt{0.25(w_2 - w_1)^2 + L^2}}{(w_1 + w_2)L + 2h\sqrt{0.25(w_2 - w_1)^2 + L^2}} = 0.037, \tag{8}$$

and thus negligible.

For the channels of Type A and B, the ratio Φ, Eq. (8), is 0.888 and 0.426, respectively (see Table 3; the ratio for the Type D channel cannot be calculated accordingly because of the complexity of its geometry). This quantitative result obtained for channels A, B and C allows for a first conclusion: the proportion of inclined walls to the overall channel inner surface crucially affects the diode effect.

2.6 Diodicity

The diodicity $\mathcal{D}$ (Eq. 6) of each data set is plotted against Kn_{m} in Fig. 3. As it is clear from Fig. 3, the diodicity of the Type A channel (solid lines at the middle in Fig. 3) is the highest and the diodicity is lower for the channels of Type B (dot-dashed lines) and D dashed lines. The use of the same gases as CO_2 (for three channels of Type A, B and D) and N_2 (for the channels of Type A and D) preserves the same hierarchic tendency of the diodicity level: the highest for A Type channel, then D Type and finally B Type. The diodicity of the Type C channel was previously found to be

insignificant, as already indicated by Fig. 2c. In Fig. 3, we can observe again that the diodicity of Type C channel is less than 1 % for Helium, as shown by means of the solid line bottommost of Fig. 3.

2.7 Opening angle

As described in the previous section and summarized in Table 3 the parameter Φ of the various channel types respects generally the same tendency as the diodicity here above. However, the parameter Φ is not exactly known for the Type D channels. In addition, this parameter refers only to the area of the inclined surface and not at all to the strength of this inclination. That is why we define the opening angle α as a second, more significant geometric measure:

$$\alpha = atan(0.5|D_2 - D_1|/L), \qquad (9)$$

using the hydraulic diameters at the channel end sections, D_1 and D_2, respectively. Since α is involving the inclined area as well as the channel length, it expresses the taperedness of the considered channels more reliably as Φ. The opening angle allows us to describe the inclination of an arbitrarily tapered channel by one value.

The opening angles according to Eq. (9) are provided in Table 3, and they indicate that the diodicity decreases with α decreasing. We obtain here a second conclusion: the inclination of the walls determines the strength of the diode effect, and it increases with the opening angle of an arbitrarily tapered channel.

2.8 Influence of the gas nature

The results obtained on the channel of Type A allow us for the comparison of three different gases: argon, nitrogen and carbon dioxide. Here, the diodicity of the monoatomic argon is higher than that of polyatomic carbon dioxide molecule, see Fig. 3, even if the both molecules have similar molar masses, see Table 5 in "Appendix" section. For nitrogen, having a lower molar mass, but a less complex structure than that of CO_2, the diode effect lies below that of Ar, and yet above that of CO_2. The same tendency is found for the results obtained on the Type D channel: the diodicity of N_2 is higher than that of carbon dioxide. However, the diodicity of the N_2–H_2 mixture, which has an average molar mass of $\mathcal{M} = 0.015$ kg/mol, is significantly lower than those of the two other test gases, nitrogen and carbon dioxide. The results of Type B channel allow for the comparison of CO_2 and the monoatomic and eleven times lighter He: the diodicity of the latter is distinctly lower.

All these observations indicate that the molar mass and the internal structure of the impinging molecules have an influence on the diode effect. This tendency may be pointed out as a third conclusion: a high molecular mass and a monoatomic structure of the gas molecules promote the diode effect. In addition, pointing out in the same direction, it was observed previously, Gronych et al. (2004), Graur et al. (2009), Yamaguchi et al. (2011), Perrier et al. (2011b), that in the case of monoatomic gases, the accommodation coefficient decreases when the atomic mass of the gas increases.

This statement, however, cannot be extended to the polyatomic molecules. For instance, it is not clear why the diodicity of nitrogen is higher than that of carbon dioxide while the molar mass of the latter one is approximately 1.5 times higher. Probably the complex polyatomic structure modifies the spherical behavior of the monoatomic gases during the collision with the wall and so doing, diminishes the specular character of the reflection.

3 Some provisional conclusions

From the previous experiments and analysis, we have derived three provisional conclusions along Sects. 2.5, 2.7 and 2.8. The first and second ones concern the geometrical aspects of the channel, while the third is related to the gas nature. All conclusions finally concern the wall properties and may be recalled here above in three points:

1. The proportion of inclined internal walls to the overall channel internal surface crucially affects the diodicity.
2. The inclination of the wall determines the strength of the diode effect. While an uniform channel (non-inclined walls) does not show any diodicity, this effect should increase with wall inclination, i.e., with increasing opening angle of the tapered channel defined in Sect. 2.7. This conclusion is not redundant with the first one, because as explained in Sect. 2.7, the opening angle defines more completely the importance of the non-straight character of the tapered channel.
3. The molecular mass and, to some extent, the nature (number of atoms, molecular diameter) of the colliding gas molecules should have an impact on the diode effect. We notably found that in case of the monoatomic gases, a high molecular mass promotes the diode effect. Furthermore, in Sect. 2.8, we explain why we may say correlatively that a decreasing accommodation of the gas momentum at the wall increases the diode effect.

These comments suggest that the wall surfaces play a major role in the diode effect genesis; this wall influence seems to occur through the slip boundary conditions, the
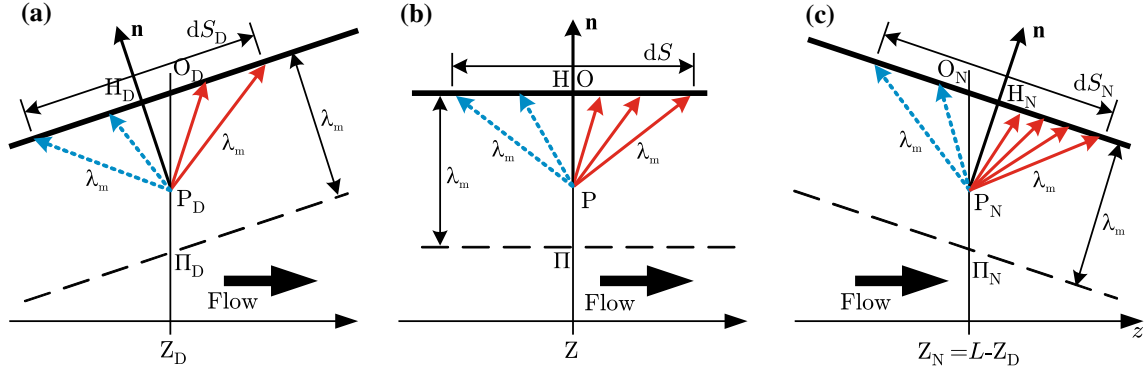
Fig. 4 Comparison of the number of potential collisions at the wall for molecules passing a point P in diffusor direction [diverging channel; marked (D)] (**a**), uniform channel (**b**), and nozzle direction [converging channel; marked (N)] (**c**). The flow is considered in the positive z-direction. *Colored arrows* represent the molecules incoming directly at the wall: *red* on the *right* (*solid lines*) from the normal direction, *blue* on the *left* (*dashed lines*). The choice of unique λ_m corresponds to simplified description given in Sects. 4.1 and 4.2

accommodation and the reflection processes at the wall. In the following section, we present corresponding physical comments on the diode effect.

4 Comments on the diode effect physics

We explain the experimentally observed diode effect by means of the gas–wall interactions and the slip boundary conditions at the wall. This approach is suggested by the fact that the phenomenon does neither appear in the hydrodynamic (no-slip) flow regime, nor in the free molecular regime. This hypothesis is strengthened by the observation that the diodicity increases with the proportion of inclined inner surface and with the opening angle (see Sect. 3). This mechanism is first analyzed in an uniform channel and then adapted to tapered channels.

4.1 Uniform channel

As a reference, we first consider a uniform channel of length L with a constant cross section A, see Fig. 4b. A gas flows through this channel in the positive direction of the z axis, driven by the difference of pressure $(p_1 - p_2)$. We assume that the Knudsen number, Eq. (1), is relatively large, so that a slip velocity exists at the wall.

Let us consider A being located at the position Z as shown in Fig. 4b. In this section, we virtually draw a line of points P parallel to the wall at a distance OP, smaller or equal to a mean free path of the molecules λ_m, Eq. (2). Now, we define an incremental surface area, dS, associated with any point P. This dS surface is proportional to the channel width w. Its dimension along the flow direction is limited in such a way that the molecules, coming from any

point P, could impinge on dS directly, i.e., without colliding with another molecule (see the arrows in Fig. 4b with a maximal length equal to λ_m). Thus, any surface increment dS is very close to a rectangular spherical sector having a ray close to the mean free path and centered around P. Therefore, the dS area is practically equal to $K\lambda_m w$, where K depends on the relative location of P along the section line $K \sim PO/\Pi O$ (see Fig. 4).

In order to describe the molecule–wall interactions, we adopt the diffuse-specular Maxwellian model. By that, the collisional exchange at the wall may be described as follows:

- in the diffuse reflection, only the incoming molecule velocities contribute to the slip;
- in the specular reflection, the contribution to the slip is due to the incoming and reflected velocities.

It is important now to differentiate the wall collisions on the right of the ZO normal line from those on the left. Indeed, for any molecule impinging on the right, its tangential component along the wall is in the sense of the flow, but for any molecule colliding on the left, its tangential momentum is directed against it.

From a geometrical point of view, the numbers of molecule–wall collisions on the left and on the right would be the same. However, due to the superimposed flow velocity the collision frequency on the right of the ZO line is higher than on the left. This same scenario may be repeated for each point P of the section ranging between the distances λ_m and zero from the wall. Moreover, this balancing may be repeated at every section of the channel.

Considering those comments, this local collision balance leads to the presence of a velocity component tangent to the wall in the positive sense of the macroscopic flow.

4.2 Tapered channels

Now, let us compare the nozzle and diffusor configurations of a tapered channel (Fig. 4a, c). In each configuration, we choose the cross section A_N and A_D with the same area ($A_N = A_D$), located, respectively, at the positions Z_N and $Z_D = L - Z_N$ on the z axis. In these sections, we consider the points P (P_N and P_D) as defined for the uniform channel. But now, we consider the center points H_D and H_N of dS_D and dS_N, respectively, aside of O_N and O_D, respectively (see Fig. 4a, c). In addition, we have to specify the points P_N and P_D as "corresponding" if their relative locations $K \sim PO/\Pi O$ are the same along their respective ΠO lines ensuring the same value of K, see Sect. 4.1 and Fig. 4.

Let us note that, in this paragraph, we admit provisionally a simplifying approximation of the pressure distribution along the channels: precisely, we consider that the diffusor pressure p_D at position Z_D is the same as the nozzle pressure p_N at position Z_N, and we describe some features of the flow under this hypothesis. In Sect. 4.3, we will discuss the effect of this assumption.

Thus, under this simplified assumption, the numerical densities n_N and n_D at the corresponding points P are the same, as well as the same mean free paths λ_m ($\Pi_N O_N = \Pi_D O_D$) in the considered cross sections A_N and A_D. Moreover, due to this last relation, the "corresponding" points locations verify $O_D P_D = O_N P_N$. Finally, the dS corresponding elementary surfaces have the same area, $dS_D = dS_N$, what simplifies the wall exchange comparison. Furthermore, following the zero-order approach using the Knudsen number (i.e., the hydrodynamic approximation) the mass flow rates are the same in the both configurations. Hence, and in the respective equal sections A_N and A_D, we obtain the same mean flow velocity. This description suggests that the macroscopic parameters are very close in these "corresponding" sections, and their difference is located close to the wall and is due to the molecule–wall collisions. Now, we can evaluate the effect of the respective reflections and momentum exchanges at the wall for each configuration.

As mentioned in Sect. 4.2, the collision frequency on the right-hand side of the normal lines PH is higher for any configuration due to the presence of the mean flow velocity. For that reason, the molecule–wall collisions are more frequent in the nozzle configuration and less frequent in the diffusor configuration. Indeed, the molecules coming from P are not spatially distributed around P in a uniform manner. If anything, they are influenced by the mean direction of the flow: the more of the observed incoming molecule direction will be close to the mean direction of the flow, the more important will be the considered molecular flux. In greater detail, on Fig. 4 the impinging directions defined by the dS_N surface and the point P_N are closer to the flow

direction than those of the corresponding molecule directions defined by the dS_D surface and the point P_D. This feature occurs for all reflection processes (diffuse and specular), and it is more significant on the right of the respective normal lines PH. Thus, if we define R^0 as the ratio between the flux of molecules impinging dS_N directly from P_N and the flux of molecules impinging dS_D from P_D, we recognize that

$$R^0 \geq 1. \tag{10}$$

From those considerations, we can conclude that, under the assumed conditions, the nozzle configuration tends to increase the velocity slip stronger and favors the macroscopic mass flow rate.

Two important remarks may be added, based on the incoming molecules distribution around the mean flow direction, previously commented.

- The impinging molecule flux at the wall in the uniform channel is more important than in the diffusor and less important than in the nozzle channel, conversely to the angle observed between the mean direction of molecule incoming on dS and the mean direction of the flow.
- The vanishing diode effect in free molecular regime may be related to smaller influence of the mean flow direction: indeed, the pressure decreases leading to a smaller influence of the molecule–molecule collisions. Correlatively the influence of the bulk velocity on the distribution of the incoming molecules vanishes. Then, the various geometrical configurations and their respective angles have a minor importance.

4.3 Influence of a realistic pressure profile

In the previous description, we omitted that the pressures are different at the considered sections A_D and A_N. The numerical results in Ref. Szalmas et al. (2015) show a pressure distribution along the diffusor direction clearly smaller than that along the nozzle direction.

Therefore, we have to estimate how the fluxes of molecules impinging on dS should be modified. First, let us note that such exchanged flux obviously depends proportionally on two factors:

- the number densities at P_N or P_D (n_N or n_D). In the previous Section, we assumed $n_N = n_D$;
- the probability that such molecules impinge dS directly, i.e., the surface areas dS_D or dS_N themselves.

Furthermore, the dS area values have been evaluated in the previous Sections as $dS = K\lambda_m w$. Here the mean free path λ_m changes according to the configurations from λ_{m_D} to λ_{m_N}. But P_D and P_N remain defined as

"corresponding" points, see Sect. 4.2: the surface ratio reduces to $dS_N/dS_D = \lambda_{m_N}/\lambda_{m_D}$. From these comments and Eq. (10), the new ratio of collision numbers reads $R = R^0(\lambda_{m_N}/\lambda_{m_D})(n_N/n_D)$.

For isothermal conditions, however, $\lambda_{m_N}/\lambda_{m_D}$ equals n_D/n_N and the correcting factors reduce to 1 and $R = R^0$. Finally, the changes in the pressure distribution do not modify the ratio of the respective collision numbers. Therefore, the nozzle configuration actually favors a higher slip velocity and consequently a greater mass flow rate.

5 Conclusion

In this work, we present an experimental campaign regarding four tapered test channels of various geometrical shapes and using various gases. Here we can show that the diode effect crucially depends on the proportion of inclined walls to the overall channel inner surface Φ. Also the inclination of the wall determines the strength of the diode effect meaning that the diodicity $\mathcal{D}$ increases with the opening angle α. Furthermore, we found that molar mass and internal structure of the impinging molecules have an influence on the diodicity: a high molar mass in a monoatomic structure of the gas molecules promotes the diode effect. A comprehensive experimental campaign to study the influences of the polyatomic molecular structure on the diode effect is not carried out yet, but should be considered for future work.

From the obtained results, we deduce and propose a consistent physical explanation of the gas flow diode effect that is mainly based on the reflection process of gas molecules colliding with the inclined walls of a tapered channel. We explained the diodicity in the framework of the Maxwellian diffuse-specular reflection on the wall. It is known, however, that this model of the molecule–wall interaction is not complete and cannot distinguish accommodation of tangential momentum from accommodation of energy, which the more complex model of Cercignani-Lampis does. Nevertheless, for the consideration of isothermal flows, the interpretation of the diode effect by means of the Maxwellian diffuse-specular model is completely satisfactory.

An alternative way to study the gas flow diode phenomenon could be the use of DSMC simulation with the separated collision and ballistic parts as it was done in Vargas et al. (2014), Reinhold et al. (2014), Tatsios et al. (2015).

Appendix

See Tables 4 and 5.

Table 4 Formulas for calculating channel properties at position $i = 1, 2$ (see Fig. 1)

Channel	Cross section A_i	Perimeter P_i	Hydraulic diameter D_i
Type A	$w_i h_i$	$2(w_i + h_i)$	$2w_i h_i/(w_i + h_i)$
Type B			
Type C			
Type D	$0.5(w_{i,1} + w_{i,2})h_i$	$2\sqrt{h_i^2 + 0.25(w_{i,1} - w_{i,2})^2} + w_{i,1} + w_{i,2}$	$\frac{2(w_{i,1}+w_{i,2})h_i}{2\sqrt{h_i^2+0.25(w_{i,1}-w_{i,2})^2}+w_{i,1}+w_{i,2}}$

Table 5 Properties of gases used for experiments

Gas	$\mathcal{M}$ (kg/mol)	μ_{ref} (10^{-5} Pa s)	ω (–)	k_λ (–)
H_2	0.002	0.845	0.67	0.779
He	0.004	1.865	0.66	0.786
N_2	0.028	1.656	0.74	0.731
Ar	0.040	2.117	0.81	0.684
CO_2	0.044	1.380	0.93	0.607

Values for μ_{ref} and ω are taken from Bird (1994). k_λ is calculated as $(7 - 2\omega)(7 - 2\omega)/(15\sqrt{\pi})$ from the variable hard sphere model Bird (1994)

References

Arkilic EB, Breuer KS, Schmidt MA (2001) Mass flow and tangential momentum accommodation in silicon micromachined channels. J Fluid Mech 437:29–43

Aubert C, Colin S, Caen R (1998) Unsteady gaseous flows in tapered microchannels. In: Technical Proceedings of the 1998 International Conference on Modeling and Simulation of Microsystems, vol. chapter 11: Applications: Microfluidics (pp 486–491). ISBN:0-96661-35-0-3

Barisik M, Beskok A (2014) Scale effects in gas nano flows. Phys Fluids 26:052003

Bird GA (1994) Molecular gas dynamics and the direct simulation of gas flows. Oxford Science Publications, Oxford University Press Inc., New York

Cercignani C (1990) Mathematical methods in kinetic theory. Premuim Press, New York

Ewart TP, Perrier P, Graur IA, Meolans JG (2006) Mass flow rate measurements in gas micro flows. Exp Fluids 41:487–498

Ewart TP, Perrier P, Graur IA, Meolans JG (2007) Tangential momemtum accommodation in microtube. Microfluid Nanofluidics 3:689–695

Ewart T, Perrier P, Graur IA, Méolans JG (2007) Mass flow rate measurements in microchannel, from hydrodynamic to near free molecular regimes. Fluid Mech 584:337–356

Franssila S (2010) Introduction to microfabrication, 2nd edn. Wiley, Chichester

Graur I, Ho MT (2014) Rarefied gas flow through a long rectangular channel of variable cross section. Vacuum 101:328–332

Graur IA, Méolans JG, Zeitoun DE (2006) Analytical and numerical description for isothermal gas flows in microchannels. Microfluid Nanofluidics 22:64–77

Graur IA, Perrier P, Ghozlani W, Méolans JG (2009) Measurements of tangential momentum accommodation coefficient for various gases in plane microchannel. Phys Fluids 21:102004

Graur I, Veltzke T, Meolans JG, Ho M, Thöming J (2015) The gas flow diode effect: theoretical and experimental analysis of moderately rarefied gas flows through a microchannel with varying cross section. Microfluid Nanofluidics 18:391–402

Gronych T, Ulman R, Peksa L, Repa P (2004) Measurements of the relative momentum accommodation coefficient for different gases with a viscosity vacuum gauge. Vacuum 73:275–279

Hemadri V, Varade V, Agrawal A, Bhandarkar UV (2016) Investigation of rarefied gas flow in microchannels of non-uniform cross section. Phys Fluids 28:022007

Knudsen M (1909) Die Gesetze der Molekularströmung und der inneren Reibungsströmung der Gase durch Röhren. Ann Phys 333:75–130

Lund LM, Berman AS (1966a) Flow and self-diffusion of gases in capillaries. J Appl Phys 37:2489–2495

Lund LM, Berman AS (1966b) Flow and self-diffusion of gases in capillaries. J Appl Phys 37:2496–2508

Marino L (2009) Experiments on rarefied gas flows through tubes. Microfluid Nanofluidics 6:109–119

Méolans JG, Nacer MH, Rojas M, Perrier P, Graur I (2012) Effects of two transversal finite dimensions in long microchannel: analytical approach in slip regime. Phys Fluids 24(11)

Perrier P, Graur IA, Ewart T, Meolans JG (2011a) Mass flow rate measurements in mircotubes: from hydrodynamic to near free molecular regime. Phys Fluids 23:042004

Perrier P, Graur IA, Ewart T, and Méolans JG (2011b) Mass flow rate measurements in microtubes: from hydrodynamic to near free molecular regime. Phys Fluids 23(4)

Reinhold J, Veltzke T, Wells B, Meierhofer Schneider J, Colombi Ciacchi L, Chaffee A, Thöming J (2014) Molecular dynamics simulations on scattering of single Ar, N_2, and CO_2 molecules on realistic surfaces. Comput Fluids 97:31–39

Rojas-Cardenas M, Graur I, Perrier P, Méolans JG (2013) Time-dependent experimental analysis of a thermal transpiration rarefied gas flow. Phys Fluids 25:0072001

Sharipov F (1999) Rarefied gas ow through a long rectangular channel. J Vac Sci Technol A 17(5):3062–3066

Sharipov F, Bertoldo G (2005) Rarefied gas flow through a long tube of variable radius. J Vac Sci Technol A 23:531–533

Sharipov F, Seleznev VD (1994) Rarefied gas flow through a long tube at any pressure ratio. J Vac Sci Technol A 12(5):2933–2935

Sharipov F, Seleznev V (1998) Data on internal rarefied gas flows. J Phys Chem Ref Data 27(3):657–706

Steckelmacher W (1986) Knudsen flow 75 years on: the current state of the art for flow of rarefied gases in tubes and systems. Rep Prog Phys 49:1083–1107

Szalmas L, Veltzke T, Thöming J (2015) Analysis of the diodic effect of flows of rarefied gases in tapered rectangular channels. Vacuum

Tatsios G, Stefanov S, Valougeorgis D (2015) Predicting the knudsen paradox in long capillaries by decomposing the flow into ballistic and collision parts. Phys Rev E 91(061001(R))

Titarev VA, Utyuzhnikov SV, Shakhov EM (2013) Rarefied gas flow into vacuum through square pipe with variable cross section. Comput Math Math Phys 53(8)

Varade V, Duryodhan V, Agrawal A, Pradeep AM, Ebrahimi A, Roohi E (2014) Low mach number slip ow through diverging microchannel. Comput Fluids 111:46–61

Varade V, Agrawal A, Pradeep AM (2015) Slip flow through a converging microchannel: experiments and 3D simulations. J Micromech Microeng 25:025015

Vargas M, Tatsios G, Valougeorgis D, Stefanov S (2014) Rarefied gas flow in a rectangular enclosure induced by non-isothermal walls. Phys Fluids 26:157101

Varoutis S, Naris S, Hauer V, Day C, Valougeorgis D (2009) Computational and experimental study of gas flows through long channels of various cross sections in the whole range of the Knudsen number. J Vac Sci Technol A 27:89–100

Velasco AE, Friedman SG, Pevarnik M, Siwy ZS, Taborek P (2012) Pressure-driven flow through a single nanopore. Phys Rev E 86:025302

Veltzke T (2013) On gaseous microflows under isothermal conditions. Ph.D. thesis, University of Bremen

Veltzke T, Baune M, Thöming J (2012) The contribution of diffusion to gas micro flow: an experimental study. Phys Fluids 24:082004

Wilke CR (1950) A viscosity equation for gas mixture. J Chem Phys 18:517–522

Yamaguchi H, Hanawa T, Yamamoto O, Matsuda Y, Egami Y, Niimi T (2011) Experimental measurement on tangantial momentum accommodation coefficient in a single microtube. Microfluid Nanofluidics 11(1):57–64

Yamaguchi H, Rojas-Cardenas M, Perrier P, Graur I, Niimi T (2014) Thermal transpiration flow through a single rectangular channel. J Fluid Mech 744:169–182